



Metal loaded WO₃ particles for comparative studies of photocatalysis and electrolysis solar hydrogen production

G.W. Ho^{a,*}, K.J. Chua^b, D.R. Siow^a

^a Department of Electrical and Computer Engineering, National University of Singapore, 4 Engineering Drive 3, Singapore 117576, Singapore

^b Department of Mechanical Engineering, National University of Singapore, 10 Kent Ridge Crescent, Singapore 119260, Singapore

ARTICLE INFO

Article history:

Received 3 October 2011

Received in revised form 8 December 2011

Accepted 10 December 2011

Keywords:

Hydrogen

Water-splitting

Photoelectrochemical

Electrolysis

Tungsten oxide

ABSTRACT

Striving for new solar hydrogen fuel, the water oxidation reaction based on photocatalyst suspension and photoelectrochemical (PEC) cell are currently the most important research for sustainable energy. Here, the effects of electrolyte pH, crystallinity and grain size of tungsten trioxide (WO₃) particles on photoconductivity are studied. Subsequently, a simple hydrothermal route was employed to synthesize Cs loaded WO₃ (Cs-WO₃) particles to further improve the photochemical reactivity. The photoanodes and photocatalyst based on the Cs-WO₃ reveals a different photoreactivity performance in the PEC and photocatalyst suspension systems. This important fundamental insight can assist in optimization of WO₃ particles photocatalyst and photoanode for future hybrid photocatalysis–electrolysis water splitting system. Based on the high photocatalytic capability demonstrated in this study, surface modified WO₃ particles are proven to be a promising candidate for efficient water-splitting catalyst.

© 2012 Elsevier B.V. All rights reserved.

1. Introduction

The earth is well positioned to produce an unlimited supply of clean hydrogen fuel as there is ample supply of sunshine and water. The need for energy sustainable development without emitting carbon or contributing nuclear waste, compels scientist and engineers to develop clean energy solutions dependent on solar energy. In order to overcome the intermittency of sun radiation, it is essential to create a material to be able to capture, convert and store. Undoubtedly, the most attractive method for this solar conversion and storage is in the form of hydrogen energy carrier. Hydrogen is a clean energy carrier since the chemical energy stored is easily released when it combines with oxygen, yielding only water as the by-product. The added advantages of hydrogen are being transportable and storable for extended time.

During the last decades, a wide range of oxides is examined for use as anodes in photoelectrochemical cells for the conversion of solar energy into hydrogen [1–4]. TiO₂ [5–7], WO₃ [8,9] and Fe₂O₃ [10–12] are the most commonly studied metal oxides for photocatalytic and photoanode materials [2–12]. In addition, there are quite a number of papers that focus on WO₃ catalysts for photodegradation work [13–17]. These oxides possess physical and chemical resilience toward harsh environments such as continuous contact to water and solar irradiation. Moreover, they are relatively

abundance in nature. The theoretical solar-to-hydrogen (STH) efficiency under solar Air Mass 1.5 Global illumination taking into account of only the bandgaps, Fe₂O₃ (STH efficiency 15%, bandgap 2–2.2 eV), monoclinic WO₃ (10.6%, 2.5–2.9 eV) and anatase TiO₂ (2.9%, 3.2 eV) [18]. Although Fe₂O₃ has the lowest bandgap, it typically suffer from a large positive photocurrent onset potential (ca. 0.8 V versus the reversible hydrogen electrode), which requires the application of additional electric bias in water splitting reaction. In the case of WO₃, sometimes expressed as WO_{3-x} (x = 0–1), bandgaps ranging from 2.5 to 3.0 eV, depending on their stoichiometries, crystalline structures and defects. WO₃ is a promising candidate for stable visible-light driven photocatalyst, including a deeper valence band and strong absorption within the solar spectrum [19–21]. However, pure WO₃ has lower light energy conversion efficiency compared to TiO₂ since the reduction potential is relatively low [22]. Thus several strategies including surface and interface modification, composite materials, transition/noble metal doping, surface sensitization have been adopted to enhance the photocatalytic properties. In particular, the limitation of WO₃ as a photocatalyst can be compensated for by modifying the morphology and surfaces of the semiconductor. Metal–semiconductor modifications are used primarily to increase electron trapping, inhibit charge recombination and increase the selectivity of a particular product so as to improve efficiency of photocatalytic processes.

Here in this paper, we investigate the effect morphology and surface modification by annealing and metal loading of WO₃ particles on photocatalysis and photoelectrolysis performance.

* Corresponding author. Tel.: +65 6516 8121; fax: +65 6775 4710.

E-mail address: elehgw@nus.edu.sg (G.W. Ho).

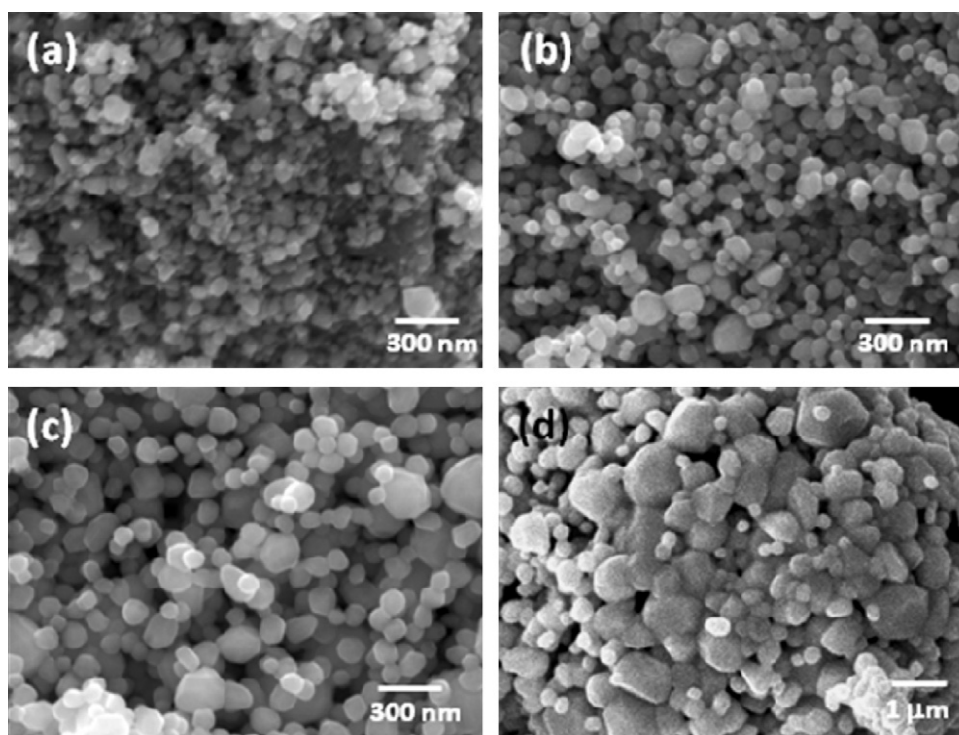


Fig. 1. SEM images of WO_3 particles (a) as prepared, (b) 600, (c) 700 and (d) 800 °C. The diameters of the particles increase with annealing temperature.

The comparative results clearly suggest a different charge transport mechanism present in the two photoreactivity systems. This important fundamental insight can assist in optimization of WO_3 particles photocatalyst and photoanode for future hybrid photocatalysis–electrolysis water splitting.

2. Experimental procedure

WO_3 nanopowder (<100 nm), cesium carbonate (Cs_2CO_3), polyethylene glycol (PEG) $M_w = 20,000$, potassium hydroxide (KOH) pellets were purchased from Sigma–Aldrich. All of the chemicals are of analytically grade purity and were used without further purification. WO_3 particles were transferred into Teflon-lined autoclaves with de-ionized (DI) water and 2.43 mM Cs_2CO_3 aqueous solution. The hydrothermal treatment was conducted at 120 °C for 12 h before the suspension was rinsed and dried for further use. Scanning Electron Microscope (SEM) micrographs of the particles were obtained using a JEOL JSM-7001F at 10 kV. Structural characterizations were obtained by X-ray diffraction (XRD) on Philips X-ray diffractometer with $\text{CuK}\alpha$ radiation. The absorption spectra of the films were recorded using a Shimadzu UV-3600 spectrophotometer.

All the photoactivities were performed from a side-window quartz tube. A 250 W mercury lamp with wavelength illuminator at 365–550 nm was employed for UV to visible light irradiation with the samples placed 50 mm away from the lamp. The photoelectrochemical measurements of the films were carried out using WO_3 particles as the photoanode and Pt as the counter electrode. Various treated WO_3 particles were mixed with PEG at 1:1 mass to form a smooth paste. Thin films were doctor bladed on SnO_2 :F-coated conducting glass as the photoanodes. The coated films were annealed in air at 450 °C for 1 h. The counter-electrodes used were Pt coated SnO_2 :F conducting glass. As for the photocatalyst suspension system, the photocatalyst powder (0.01 g) was dispersed in 10 ml of $\text{Fe}_2(\text{SO}_4)_3$ aqueous solution. Photocatalytic decomposition of water through a new reaction mechanism, similar to the

Z-scheme reaction was carried out using WO_3 particles catalyst and Fe ion redox system. The suspension was stirred vigorously using a magnetic stirrer to ensure homogeneous mixture. Next, all the experiments involved purging of the reactor quartz tube with N_2 for 15 min before illumination of light. The amount of evolved H_2 was determined using gas chromatography HP 6890 Series G1530A, thermal conductivity detector with N_2 carrier.

3. Results and discussion

Fig. 1 shows morphologies of the WO_3 particles at different annealing temperatures. The particles are generally spherical in shape and have a fairly tight size distribution. The average diameter of the particles increases with annealing temperature. The average diameter for the as-prepared particles is ~80 nm (**Fig. 1a**). Annealing the samples increases the mean particle size to 130, 190 and 900 nm for 600, 700 and 800 °C (**Fig. 1b–d**). A huge increase in mean particle diameter is observed between 700 and 800 °C. The primary particles appear to have agglomerated and sintered to form large crystallites, some are more than 1 μm in diameter. The surfaces of these large crystallites appear smooth and fairly faceted. The sintering and interconnection of the WO_3 particles is considered a desirable aspect for enhanced electron conductivity.

The XRD patterns for WO_3 films annealed at different temperatures are shown in **Fig. 2**. The diffraction peaks indicated the presence of monoclinic WO_3 phase, according to JCPDS data (JCPDS 43-1035). The monoclinic WO_3 phase exhibits three characteristic peaks at $2\theta = 23.3$, 23.8, and 24.6° and is the most stable phase at room temperature. These peaks of the various spectra are relatively similar in intensity which suggests no preferential crystal growth direction. However, there is a distinct increase in intensity and sharpening of diffraction peaks with increase annealing temperature, most likely attributed to the improved crystallinity. The full-width-half-maximum (FWHM) of the (001) crystal plane of monoclinic WO_3 decreases with increasing annealing temperature. The decrease of FWHM is in coherent with the

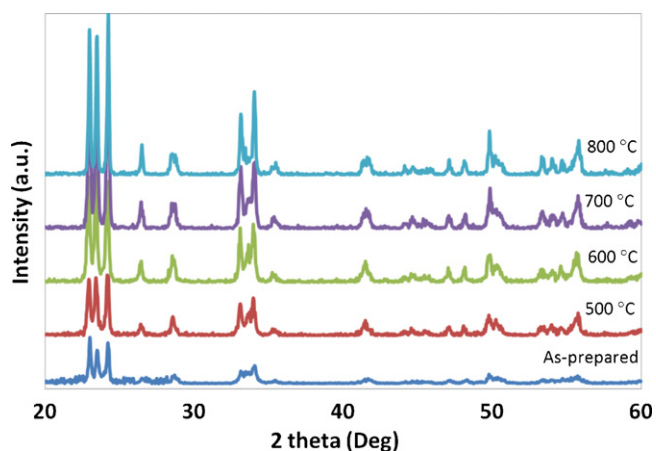


Fig. 2. XRD spectra of WO₃ particles, as prepared and annealed at various temperatures. The crystallinity and grain size increase with annealing temperature.

Debye–Scherrer equation of grain size enlargement due to high temperature agglomeration and sintering of particles. Xin et al. have reported that the phase of WO₃ is the major influencing factor for photocatalytic activity, and that the monoclinic phase has the highest photocatalytic reaction [23].

Fig. 3 displays UV–vis diffuse reflectance spectra of various WO₃ films. The absorption onset wavelengths of the WO₃ particles vary around 450–470 nm. As the calcination temperature increases, the absorption edge is red-shifted to the long-wavelength region. The

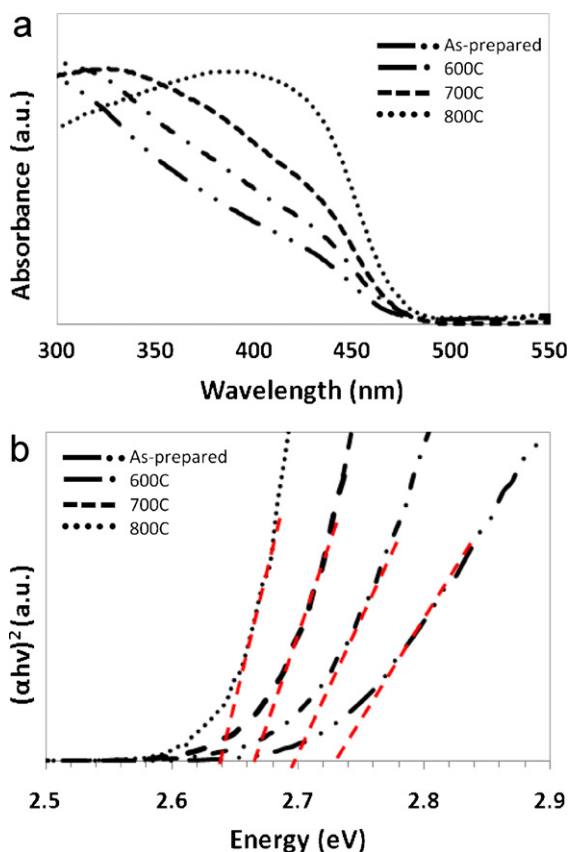


Fig. 3. (a) UV–vis spectra and (b) Tauc plot of WO₃ particles, as prepared and annealed at various temperatures.

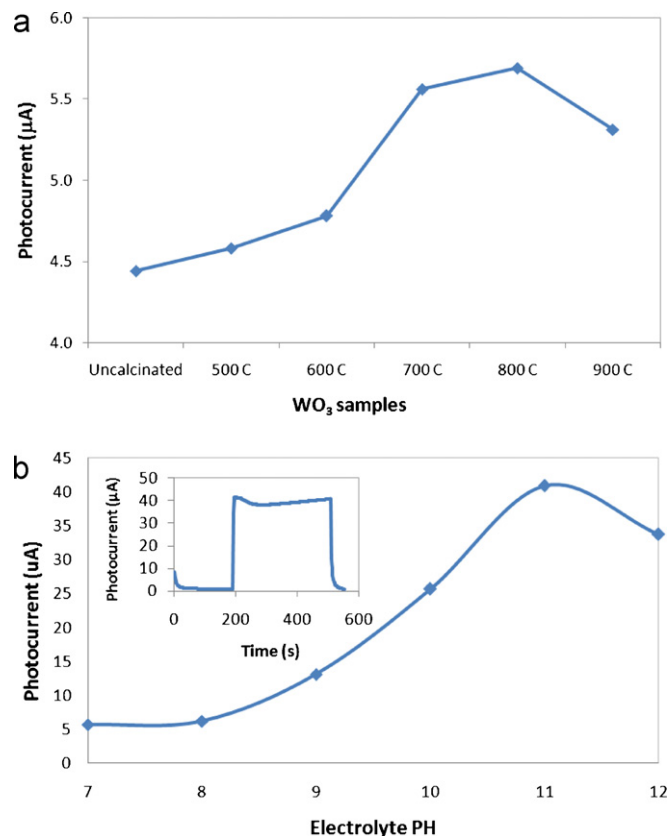


Fig. 4. Photocurrent of various (a) WO₃ particles films and (b) pH electrolyte. Inset shows the photocurrent obtained for pH 11.

absorption spectra was further analyzed by plotting $(\alpha hv)^2$ against hv , or energy, based on Eq. (1).

$$(\alpha hv)^2 = A(hv - E_g)^n \quad (1)$$

where α is the absorption coefficient, A is a constant independent from frequency ν , n is the exponent that depends upon the quantum selection rules for the particular material, and E_g is the band gap of the material. This relationship gives the E_g by extrapolating the straight portion of $(\alpha hv)^2$ against hv plot to the point $\alpha = 0$ as shown in Fig. 3b [24]. Accordingly, the as-prepared film shows band gap energy of approximately 2.73 eV, while the bulk WO₃ shows values around 3.2 eV. This result agrees with other studies reporting a bandgap energy for monocline crystalline WO₃ of approximately 2.8 eV [23]. The band gaps vary from 2.69, 2.66 to 2.64 eV with increasing annealing temperature. The red-shift of the absorption curve is accompanied by a reduction in the band gap energy as annealing temperature is increased. It is believed that the red-shift may be due to an increase in oxygen vacancy-related defects with a corresponding increase in light absorption in the long wavelength region [23]. On the basis of the above analysis, it is believed that annealing decrease the band gap and possibly facilitates response in visible light region.

Fig. 4a summarizes the photocurrents of WO₃ in the PEC cell as a function of annealing temperature. The results show that annealing of WO₃ particles increases the photocurrent of the PEC cell. This may be attributed to increase crystallinity and hence improving charge transport which directly contributes to the increase in photoconductivity. A significant increase in the photocurrent was observed between annealing temperatures of 600–700 °C. It is well-known that generation and transport of charge carriers is a rate-limiting step, hence efficient carrier transport is essential for enhanced photoconductivity. Increasing the annealing

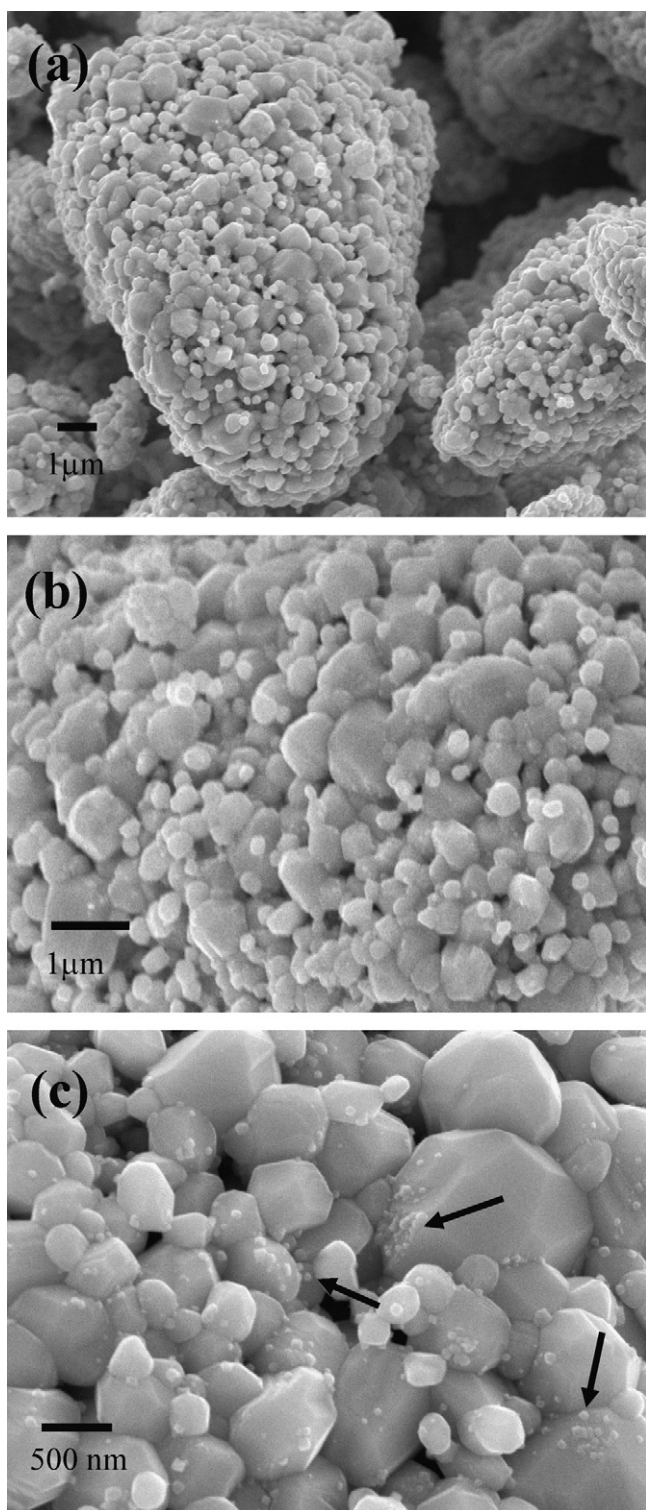


Fig. 5. Cs loaded WO_3 particles at different magnifications. The diameters of Cs crystallites are in tens of nanometers.

temperature leads to WO_3 nanoparticle agglomeration and provide better crystallographic interconnectivity, thereby improving its charge transport properties. The dominance of the monoclinic phase of WO_3 also enhances photocatalytic reactivity [23]. As the crystal grains grow in size (agglomeration) with increasing temperature, the grain boundaries along with surface recombinations are reduced. Thus, the possible factors that lead to an increase in the photocurrent are due to the improved charge transport through

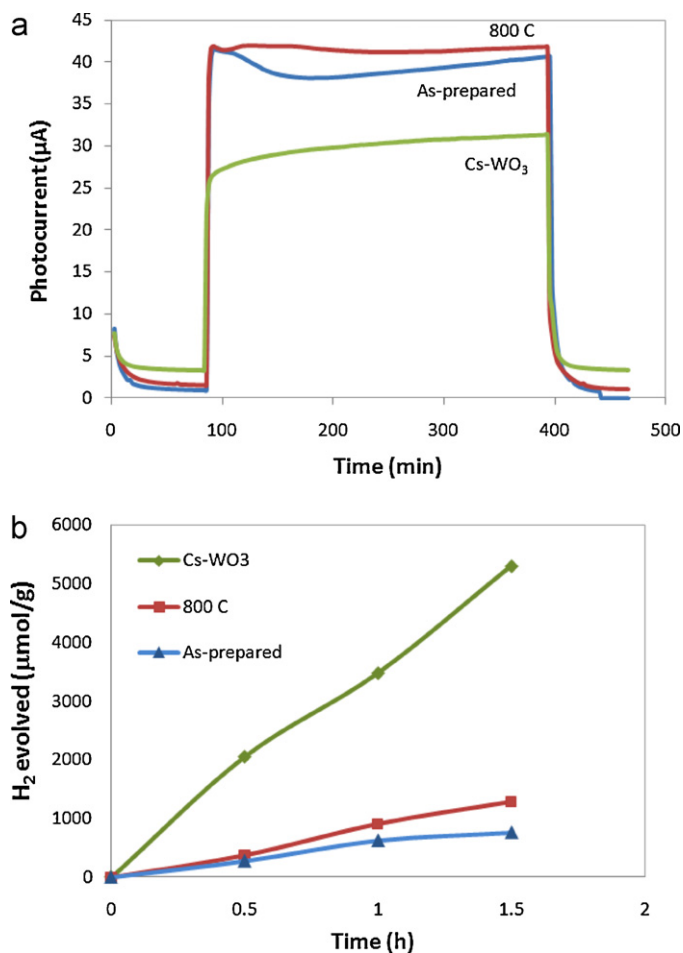


Fig. 6. Photoreactivity of various WO_3 particles samples based on (a) PEC and (b) photocatalytic suspension systems.

interconnected grains, predominant monoclinic crystalline phase and reduced surface recombinations. Further increase in annealing temperature to 900°C resulted in severe agglomeration or sintering of particles, which then compromises the surface area. This adverse effect brings about drastic reduction of specific surface area which means lesser contact with the electrolyte, thus slowing down the rate of reaction. It has been suggested by Xin et al. [23] that there is an optimum annealing temperature for improved photocatalytic reactivity, which in our present work is observed at 800°C .

Currently, most research in photocatalytic reactions has been material based. Comparatively, not much study has been done on the effects of the electrolytic environment on PEC cell efficiency. Thus, to determine the roles and effects the electrolyte has on the water splitting performance, the property pH was chosen for examination. WO_3 powder annealed at 800°C was used as the photoanode, and an external voltage bias of 1 V was applied to the PEC cell. Specifically, only alkaline pH was considered for this study, since hydroxide (OH^-) ions have a greater impact on the charge transfer reactions on the photoanode. Fig. 4b and inset shows the photocurrent of the PEC cell as a function of pH. It is observed that an increase of pH from 7 to 8 increases the photocurrent by about 9%. The effect of increasing pH on the photoconductivity is the highest between 9 and 11. The photocurrent approximately doubles for each integral increment of pH in this region. This is similar to the results obtained by Crawford et al. [25], based on TiO_2 photoanode. However, after pH 11, the photocurrent experiences a decline. This is speculated to be attributed to the instability of WO_3 in strong aqueous hydroxide solutions, since they react with OH^- ions [26].

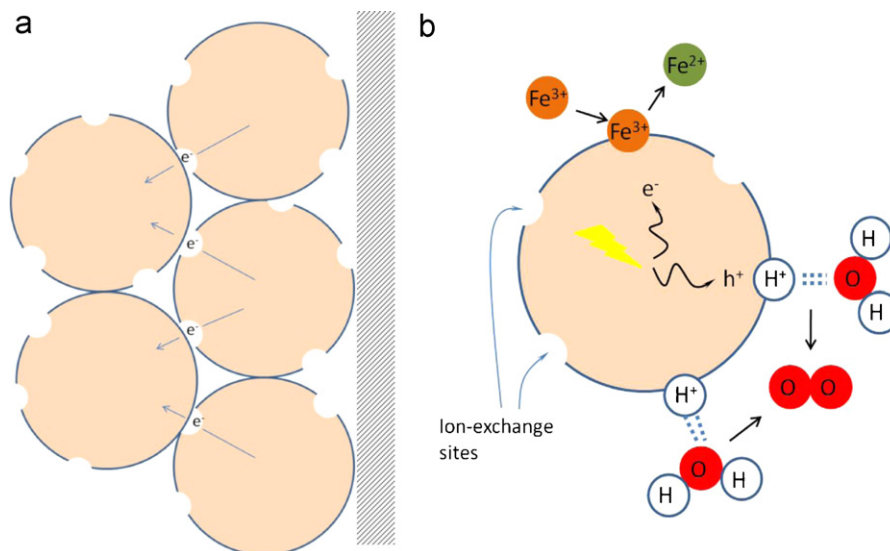


Fig. 7. Schematic diagrams of charge transport mechanisms of photoanode and photocatalyst based on (a) PEC and (b) photocatalytic suspension systems.

The effect of increasing pH (introducing OH^- ions) can be understood in terms of the reduction of overpotentials in the PEC cell and increase in conductivity of the electrolyte. In the former term, it is directly related to cell voltage efficiency. In an electrolytic cell, it refers to the additional voltage above the reversible thermodynamic potential that must be supplied to the cell in order to initiate the redox reactions. The main overpotential in the PEC cell is the transport overpotential, which is associated with the kinetic hindrance charge-transfer reaction elementary step at the electrodes [27]. The evolution of O_2 gas from the photoanode surface from oxidation of OH^- ions encounters less charge transfer overpotential, as compared to oxidation of neutral H_2O molecules. This is because OH^- ions, by virtue of their negative charge, are able to attract and trap holes in the WO_3 photoanode better than H_2O molecules. A PEC cell containing hydroxide solution as the electrolyte has greater conductivity as compared to neutral water. This is because under the influence of an electric field generated between the photoanode and the cathode, the OH^- ions are able to migrate away from the cathode toward the photoanode more efficiently than water molecules, due to their negative charge.

After the investigation and optimization of the calcination temperature of the WO_3 particles and the pH of the electrolyte, a further attempt to improve PEC cell performance was conducted. This involves hydrothermal treatment of the WO_3 powders using aqueous cesium carbonate to produce metal loaded WO_3 particles. Fig. 5 shows the SEM images of WO_3 particles after being annealed to 800°C and loaded with Cs. It is observed that the WO_3 particles retain the overall morphology with the presence of Cs nanocrystallites in the range of tens of nanometers as indicated by arrows. Three samples namely the as-prepared, heat treated (800°C) and Cs loaded WO_3 particles were tested using photocatalyst suspension and PEC systems. The photoactivity of the photocatalyst suspension system was evaluated by measuring the amount of H_2 evolution, while the PEC photoactivity of the film was determined by measuring photocurrent generation during oxidation of water. Fig. 6a shows the photocurrents of PEC cells measured using different WO_3 particles photoanodes as a function of time. The steady-state photocurrent for WO_3 with 800°C heat treatment is higher than the as-prepared WO_3 film. On the other hand, the steady-state photocurrent for Cs- WO_3 particles is significantly lower (~23–26%) than the former two samples. Fig. 6b shows the photocatalytic H_2 evolution of photocatalyst suspension system based on different WO_3 particles samples. It is noted that Cs- WO_3 film shows the

highest H_2 evolution follow by heat treated WO_3 and the as-prepared WO_3 particles. The apparent result discrepancies of the photocatalyst suspension and PEC systems based on the same material leads to the postulation that there is a difference in charge transport mechanisms between the two systems.

In a PEC cell system (Fig. 7a), photogenerated electrons travel through numerous particles within the bulk film thickness, effectively across many grain boundaries in order to contribute to the external circuit. The primary purpose of Cs- WO_3 particles film in the PEC cell is to channel the generated photoelectrons toward the conducting glass electrode. Cs ion-exchange sites on WO_3 particles will tend to trap electrons, hence disrupting the electron flow from the film to the external circuit. This also increases the chances of recombination with holes, and thus reduces the overall cell efficiency. This is unlike the photocatalyst suspension system (Fig. 7b), the redox reactions take place on the same nanoparticle itself, which means that photogenerated electrons and holes migrate from the inner bulk of the nanoparticle to the surface, where they initiate reduction and oxidation reactions, respectively. Charge separation is facilitated by the potential difference in depletion charge layer which drives photoelectrons toward the bulk and holes to the electrolyte. The Cs ion-exchange sites on the surface of the WO_3 particles helps charge separation by acting as an electron sink thus provides reaction sites. Hence these ion-exchange sites function like heterogeneous catalysts and increase the rate of water-splitting reaction.

4. Conclusions

Surface modifications in terms of heat treatment and metal loading were carried out on WO_3 particles. The crystal structure of WO_3 particles was predominantly monoclinic phases and its crystallinity and particle size increased with annealing temperature. An increase in photocurrent is demonstrated with annealing of WO_3 particles which improves the crystallinity quality, increase the grain size and reduce surface recombination loss. The photocurrent also improves with electrolyte pH due to reduction of overpotentials and increase in electrolyte conductivity. Cs- WO_3 particles show highest photoactivity in photocatalytic suspension system but lowest in the PEC system. The photoreactivity water splitting experiments in the respective photocatalytic suspension and PEC systems show that there is a stark difference in the charge transport of photoelectrons mechanisms.

Acknowledgments

This work is supported by the National University of Singapore (NUS) grant R-263-000-653-731. The authors would like to acknowledge contribution of UROP Engineering Science Programme students for the gas evolution measurements.

References

- [1] D.E. Scaife, *Solar Energy* 25 (1980) 41.
- [2] K. Rajeshwar, *J. Appl. Electrochem.* 37 (2007) 765.
- [3] A. Fujishima, K. Honda, *Nature* 238 (1972) 37.
- [4] H.H. Kung, H.S. Jarrett, A.W. Sleight, A. Ferretti, *J. Appl. Phys.* 48 (1977) 2463.
- [5] R. Asahi, T. Morikawa, T. Ohwaki, K. Aoki, Y. Taga, *Science* 293 (2001) 269.
- [6] N.K. Allam, K. Shankar, C.A. Grimes, *J. Mater. Chem.* 18 (2008) 2341.
- [7] H. Kato, A. Kudo, *J. Phys. Chem. B* 106 (2002) 5029.
- [8] B. Marsen, E.L. Miller, D. Paluselli, R.E. Rocheleau, *Int. J. Hydrogen Energy* 32 (2007) 3110.
- [9] B.D. Alexander, P.J. Kulesza, I. Rutkowska, R. Solarska, J. Augustynski, *J. Mater. Chem.* 18 (2008) 2298.
- [10] A. Kay, I. Cesar, M. Grätzel, *J. Am. Chem. Soc.* 128 (2006) 15714.
- [11] H. Dotan, K. Sivula, M. Grätzel, A. Rothschild, S.C. Warren, *Energy Environ. Sci.* 4 (2011) 958.
- [12] C.J. Sartoretti, B.D. Alexander, R. Solarska, I.A. Rutkowska, J. Augustynski, R. Cerny, *J. Phys. Chem. B* 109 (2005) 13685.
- [13] J.Y. Gong, C.Z. Yang, W.H. Pu, J.D. Zhang, *Chem. Eng. J.* 167 (2011) 190.
- [14] H.W. Choi, E.J. Kim, S.H. Hahn, *Chem. Eng. J.* 161 (2010) 285.
- [15] G. Lu, X.Y. Li, Z.P. Qu, Q.D. Zhao, H. Li, Y. Shen, G.H. Chen, *Chem. Eng. J.* 159 (2010) 242.
- [16] S.A.K. Leghari, S. Sajjad, F. Chen, J.L. Zhang, *Chem. Eng. J.* 166 (2011) 906.
- [17] S.M.A. Abdullah, F.K. Chong, *Chem. Eng. J.* 158 (2010) 418.
- [18] V. Vidyarthi, S.M. Hofmann, A. Savan, K. Sliozberg, D. König, R. Beranek, W. Schuhmann, A. Ludwig, *Int. J. Hydrogen Energy* 36 (2011) 4724.
- [19] G. Bamwenda, R.H. Arakawa, *Appl. Catal. A* 210 (2001) 181.
- [20] G. Hodes, D. Cahen, J. Manassen, *Nature* 260 (1976) 312.
- [21] D. Chen, J.H. Ye, *Adv. Funct. Mater.* 18 (2008) 1922.
- [22] Z. Xu, L.I. Tabata, K. Hirogaki, K. Hisada, T. Wang, S. Wang, T. Hori, *Mater. Lett.* 65 (2011) 1252.
- [23] G. Xin, W. Guo, T. Ma, *Appl. Surf. Sci.* 256 (2009) 165.
- [24] M.A. Butler, *J. Appl. Phys.* 8 (1977) 1914.
- [25] S. Crawford, E. Thimsen, P. Biswas, *Electrochem. Soc.* 156 (2009) H346.
- [26] E. Lassner, W.D. Schubert, *Tungsten: Properties, Chemistry, Technology of the Element, Alloys and Chemical Compounds*, Kluwer Academic/Plenum, 1999, ISBN 0-306-45053-4.
- [27] H. Dau, C. Limberg, T. Reier, M. Risch, S. Roggan, P. Strasser, *Chem. Catal. Chem.* 2 (2010) 724.